DRG-targeted helper-dependent adenoviruses mediate selective gene delivery for therapeutic rescue of sensory neuronopathies in mice

Tomoya Terashima,[1] Kazuhiro Oka,[1,2] Angelika B. Kritz,[3] Hideto Kojima,[2] Andrew H. Baker,[3] and Lawrence Chan[1,2]

[1]Department of Medicine and [2]Department of Molecular and Cellular Biology, Baylor College of Medicine, Houston, Texas, USA.
[3]British Heart Foundation Glasgow Cardiovascular Research Centre, University of Glasgow, Glasgow, United Kingdom.

Dorsal root ganglion (DRG) neuron dysfunction occurs in a variety of sensory neuronopathies for which there are currently no satisfactory treatments. Here we describe the development of a strategy to target therapeutic genes to DRG neurons for the treatment of these disorders. We genetically modified an adenovirus (Ad) to generate a helper virus (HV) that was detargeted for native adenoviral tropism and contained DRG homing peptides in the adenoviral capsid fiber protein; we used this HV to generate DRG-targeted helper-dependent Ad (HDAd). In mice, intrathecal injection of this HDAd produced a 100-fold higher transduction of DRG neurons and a markedly attenuated inflammatory response compared with unmodified HDAd. We also injected HDAd encoding the β subunit of β-hexosaminidase (Hexb) into *Hexb*-deficient mice, a model of the neuronopathy Sandhoff disease. Delivery of the DRG-targeted HDAd reinstated neuron-specific Hexb production, reversed gangliosidosis, and ameliorated peripheral sensory dysfunction. The development of DRG neuron–targeted HDAd with proven efficacy in a preclinical model may have implications for the treatment of sensory neuronopathies of diverse etiologies.

Introduction

Dysfunction of neurons in dorsal root ganglion (DRG) occurs in a variety of sensory neuronopathies (1, 2), including hereditary (3), autoimmune (4), nutritional (5), metabolic (6), and neoplastic diseases (7). DRG neuronal disorders are notoriously difficult to treat and are a common cause of much pain and suffering in the form of neuropathic pain, loss of sensation, and sensory ataxia (1, 2). Treatments that specifically target DRG neurons would be ideal. Unfortunately, the development of DRG-targeted therapy has been challenging (1, 2). Delivery of neurotrophic factors can minimize neuronal damage in the DRG (8). However, neurotrophic polypeptides are susceptible to proteolytic degeneration, and their therapeutic effects are short-lived; direct delivery of therapeutic genes proves to be more effective (9, 10). Herpes simplex virus (9) and poliovirus (11) injected through subcutaneous or intramuscular routes are taken up by endocytosis at nerve terminals, and some will travel via axonal transport to somas of DRG neurons. To further increase the efficiency of gene delivery, direct injection into DRG neurons by microneurosurgery can be accomplished by the removal of a piece of vertebra to gain access to the DRG (12, 13). However, such a maneuver is not practical for repeated injections, which is likely required for chronic disorders. In contrast, intrathecal (i.t.) injection is a far less invasive procedure that is used routinely in clinical practice (10). Nevertheless, DRG are ensheathed in the dura and bathed in cerebrospinal fluid (CSF). Gene delivery vectors could disperse and be taken up elsewhere, leading to complications, including meningitis (14). To optimize the chance for successful DRG neuron delivery while minimizing undesired off-target effects, targeted gene delivery would be an ideal strategy for delivering genes to DRG neurons (15).

Adenovirus (Ad) is an efficient gene transfer system in vitro as well as in vivo because of its capacity to infect both quiescent and proliferating cells, its broad spectrum of tissue transduction susceptibility, and the relative ease with which the vector can be produced in high titer. Helper-dependent Ad (HDAd) is the most advanced Ad, devoid of all viral coding sequences. The lack of potentially harmful Ad viral gene expression is associated with markedly reduced toxicity. HDAd-mediated in vivo gene delivery in rodents and nonhuman primates has been found to have an excellent safety profile and protracted transgene expression (16, 17). Other advantages of HDAd are a large cloning capacity, up to 37 kb, and a greatly attenuated adaptive host immune response (18). For these reasons, we selected HDAd as the backbone for the targeted vector for DRG neuron delivery.

The cellular tropism of Ad serotype 5 (Ad5) is determined by the cell surface expression of primary attachment sites coxsackie and adenovirus receptor (CAR; refs. 19, 20) and heparan sulfate proteoglycans (HSPGs; refs. 21–23). Integrins act as secondary internalization receptors (21, 24, 25). Cells deficient in the expression of these receptors are transduced with greatly reduced efficiency. Little or no CAR is expressed by DRG neurons, which are poor targets for

Conflict of interest: The authors have declared that no conflict of interest exists.

Nonstandard abbreviations used: Ad, adenovirus; CAR, coxsackie and adenovirus receptor; CSF, cerebrospinal fluid; DRG, dorsal root ganglion, dorsal root ganglia; 293-fiber cell, 293 cell expressing Ad5 wild-type fiber; βgeo, β-gal–neo fusion protein; HDAd, helper-dependent Ad; HSPG, heparan sulfate proteoglycan; HV, helper virus; i.t., intrathecal(ly); MNCV, motor nerve conduction velocity; PAS, periodic acid–Schiff; SNAP, sensory nerve action potential; SNCV, sensory nerve conduction velocity; vp, viral particle(s); WF, wild-type fiber.

Citation for this article: *J. Clin. Invest.* **119**:2100–2112 (2009). doi:10.1172/JCI39038.

Table 1
Features of modified fiber proteins

Sequence	aa Position	WF	DRG1	DRG2	DRG3	KO1S*
HSPG	91–94	KKTK	GAGA	GAGA	GAGA	GAGA
CAR	408–409	SP	EA	EA	EA	EA
Linker	542–543	None	GGSGGG	GGSGGG	GGSGGG	GGSGGG
Insert aa	NA	None	C-**SPGARAF**-C	C-**DGPWRKM**-C	C-**FGQKASS**-C	None

WF group contained Ad5 WF. All other HVs had the KO1S* backbone, which has the BspEI site (underline) within the 6-aa linker and modification of the HSPG binding site (KKTK; AAAAAAACCAAG) to GAGA (GGCGCCGGCGCC) and the CAR binding site (SP; TCTCCT) to EA (GAGGCC). The individual DRG homing peptides flanked by cysteine residues are shown in bold.

unmodified Ads (26). Considerable effort has been expended on the generation of first-generation Ads that target normally refractory tissues and retarget to alternative cell type–specific receptors. The 3 major strategies currently used are genetic modification of Ad capsid proteins; conjugation of adaptor proteins, such as antibody or bispecific fusion proteins; and chemical modification by polymers with targeting ligands (15, 27). Genetic modification appears to the most popular of these approaches. This technology is particularly appealing for HDAd because capsid proteins of HDAd are supplied by the helper virus (HV). Armed with a library of targeting HVs, one can produce HDAds that potentially target any tissue by applying the specific HV at the final amplification. To date, despite the many potential advantages of HDAds, targeting HDAds by genetic modification has been limited to the introduction of peptide ligands into the HI loop (28) or replacement of fiber gene with that of a different Ad serotype (29).

We report here a strategy to engineer fiber-modified HDAd and demonstrated the efficacy of HDAd bearing DRG neuron–specific targeting peptide (30) to correct a genetic deficiency and reverse its associated sensory deficit in a mouse model (31, 32). We introduced targeting ligands into the fiber of HV possessing mutated fiber proteins to avoid native Ad tropism and showed that these fiber-deleted HV possessed markedly impaired ability to transduce 293 cells and DRG neurons in vitro. Moreover, the addition of DRG targeting peptide ligands efficiently retargeted HV to DRG neurons. In addition, using Cre-expressing HDAd amplified in the presence of fiber-modified HVs, we documented high-efficiency DRG neuron targeting in vivo after i.t. injection into ROSA-GFP transgenic mice. Finally, we demonstrated the efficacy of the targeting strategy to correct a genetic deficiency in DRG neurons, reversing specifically the peripheral sensory nervous system dysfunction in mice with β-hexosaminidase deficiency. We suggest that this strategy, which we believe to be novel, could fill an immediate need in applying targeted HDAd gene therapy for DRG neuron disorders.

Results

Production of fiber-modified HV. In a much-used method for HDAd production, all necessary factors for packaging HDAd genome are supplied in *trans* by a HV, a first-generation Ad. In this scheme, HDAd that expresses the gene of interest (e.g., a therapeutic transgene) can be made to target a specific organ or cell type simply by using an appropriate HV at the final amplification (33) — there is no need to engineer a new HDAd (Supplemental Figure 1; supplemental material available online with this article; doi:10.1172/JCI39038DS1). To produce targeted HV, we first attenuated the natural tropism by ablating the binding sites of Ad5 fiber to ameliorate binding to primary receptors (KO1S* mutation; refs. 34, 35). To circumvent the very poor infectivity of this KO1S* mutant Ad toward 293 cells, we established 293 cells expressing Ad5 wild-type fiber (referred to herein as 293-fiber cells) to incorporate wild-type fiber (WF) into the capsid of HV-KO1S* (Supplemental Figure 3A). Fiber-modified HV generated on 293-fiber cells had both WF and modified fiber encoded by HV genome. We generated a total of 5 HVs: HV-WF; HV-KO1S*, a detargeted HV; and 3 HVs on a HV-KO1S* backbone that contain individual DRG-targeting motifs, HV-DRG1, HV-DRG2, and HV-DRG3 (Table 1, Figure 1A, and ref. 30). Fiber-modified HVs were initially generated on 293-fiber cells and subsequently amplified on 293 cells to remove WF in the final HV capsid. Proper fiber modification in the genome of individual HVs was verified by DNA sequencing (Supplemental Figure 3B).

HV containing DRG neuron–targeting motifs efficiently and specifically transduces DRG neurons in vitro and in vivo. Compared with HV-WF, HV-KO1S* showed 100-fold lower infectivity to 293 cells (Figure 1B), indicating that HV-KO1S* had lost its capacity to interact with primary docking sites on 293 cells. As the different DRG motif–containing HVs were engineered on a HV-KO1S* backbone, they also transduced 293 cells poorly (Figure 1B and Supplemental Figure 4A). In contrast, HV-DRG1–HV-DRG3 all displayed markedly enhanced transduction of isolated DRG neurons (Figure 1C). Interestingly, HV-DRG1 showed the highest transduction efficiency, followed by HV-DRG2 and HV-DRG3. Compared with HV-WF, HV-DRG1 showed 100-fold higher efficiency of DRG neuron transduction in vitro, while HV-KO1S* displayed minimal transduction capacity (less than 1% that of HV-WF, less than 0.001% that of HV-DRG1; see Supplemental Figure 4B). We next investigated the transduction efficiency of DRG neurons by the different HVs in vivo by injecting 1×10^8 viral particles (vp) of HVs containing dual β-gal–neo fusion protein (βgeo) and luciferase gene cassettes into the subarachnoid space of C57BL/6 mice and compared the biodistribution of the fiber-modified HVs 5 days later. X-gal staining was barely detectable in DRG of mice treated with HV-WF or HV-KO1S*. In contrast, transduction of DRG by HV-DRG1–HV-DRG3 was evident from X-gal staining (Figure 1D and Supplemental Figure 6C). Occasional punctate X-gal reaction product was detected in the root fibers leading to the DRG in HV-WF–treated mice. Close microscopic observation revealed rare X-gal–positive areas in the brains of mice treated with HV-WF (e.g., an X-gal–positive area was identified in the lateral ventricular region; Supplemental Figure 6A), but almost never in the brains of mice treated with other HVs. The spinal cord stained positive around the vector injection site and at the dorsal intermediate sulcus and central canal in mice treated with HV-WF. Although scant staining was found in the injection sites of mice treated with HV-DRG1–HV-DRG3, we did not observe any positive staining in mice treated with HV-KO1S* (Supplemental Figure 5 and Supplemental Figure 6B). X-gal–positive areas were also identified on the surface of the sciatic nerve in the HV-WF group, and to a much smaller extent in the HV-DRG1–HV-DRG3 groups, but not in the KO1S* group (Supplemental Figure 6D).

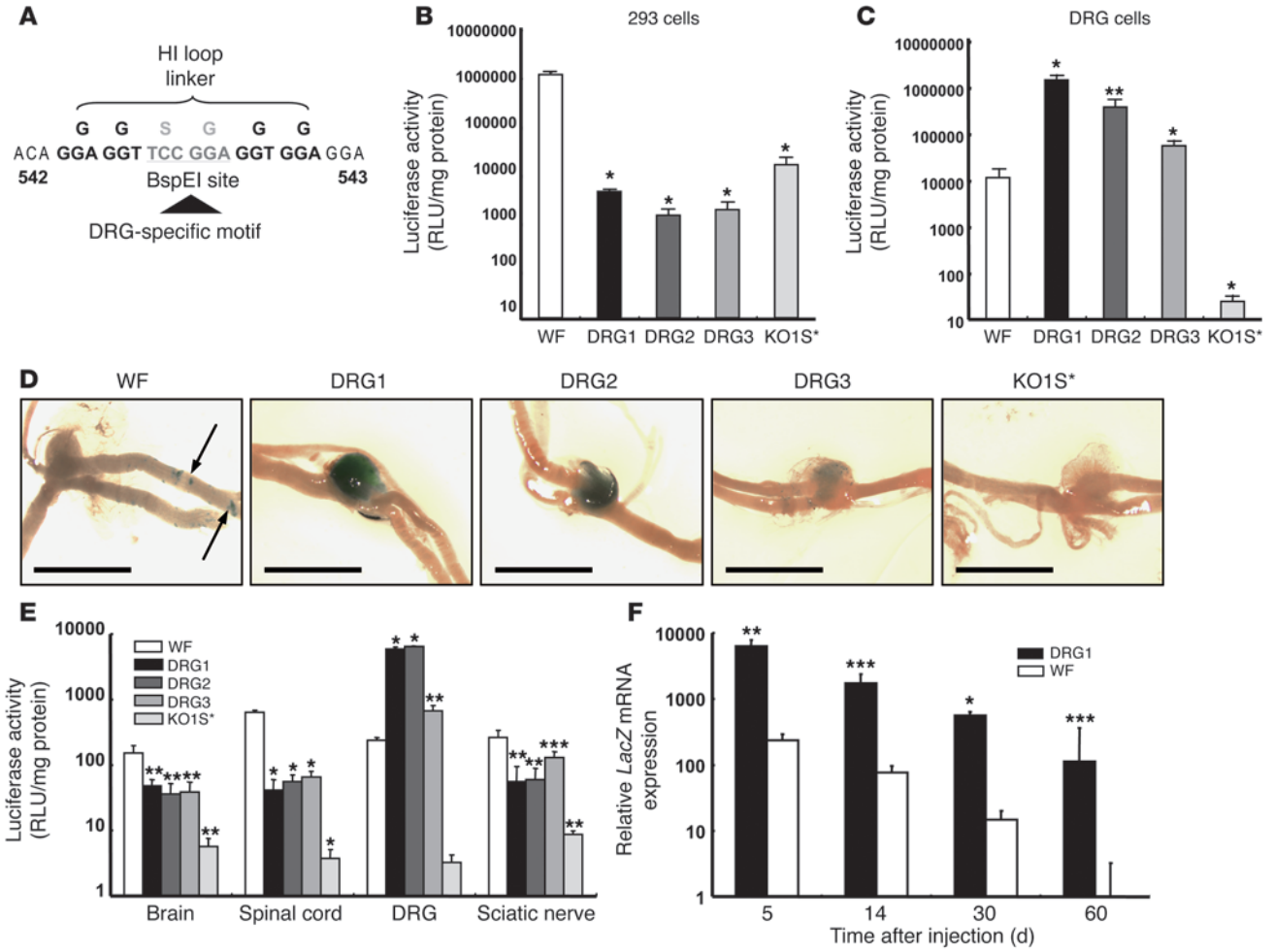

Figure 1

Transduction of DRG neurons by fiber-modified HV. (**A**) DRG homing peptides DRG1, DRG2, and DRG3 were inserted into the BspEI site in the HI loop of fiber protein. (**B**) Luciferase activity in 293 cells. Cells were infected with HVs at 1,000 vp/cell and were harvested 24 hours after infection for luciferase assay ($n = 6$). (**C**) Luciferase activity in HV-infected DRG neurons. Primary DRG neurons were infected, and luciferase activity was determined, as described in **B**. (**D**) *LacZ* expression in DRG. Fiber-modified HVs (1×10^8 vp) were injected into C57BL/6 mice through subarachnoid space at the lumbar level. Mice were sacrificed 5 days after HV injection and stained for *LacZ* expression. Arrows denote X-gal–positive areas at nerve portion. Scale bars: 2 mm. (**E**) Luciferase activities in nervous systems. Fiber-modified HVs (1×10^8 vp) were injected into C57BL/6 mice as described in **D**, and neuronal tissues were harvested 5 days after injection. (**F**) Long-term *LacZ* expression in DRG. Mice were treated with 1×10^8 vp HV-WF or HV-DRG1 and sacrificed at various times. *LacZ* mRNA in DRG was quantified by real-time RT-PCR and normalized to β-actin mRNA. Results are expressed relative to the day-60 HV-WF group. $^*P < 0.001$, $^{**}P < 0.01$, $^{***}P < 0.05$ versus WF. Note the use of log scale in **B**, **C**, **E**, and **F**.

We corroborated the observation based on X-gal staining pattern by quantifying HV-induced luciferase activity. Again, we found low luciferase activity in the HV-WF group in all tissues, whereas high luciferase activity was present almost exclusively in the DRG of HV-DRG1–HV-DRG3–treated animals. Transduction by HV-DRG1 and HV-DRG2 was 100-fold higher than that by HV-WF. HV-DRG3 was substantially less efficient, being only 4-fold higher than HV-WF (Figure 1E). Luciferase activity from HV-KO1S* (detargeted) was negligible in all tissues. We further determined long-term *LacZ* mRNA expression induced by HV-WF and HV-DRG1 by quantitative RT-PCR. The expression of *LacZ* mRNA decreased over time in both groups (Figure 1F). By 60 days, *LacZ* mRNA was barely detectable in the HV-WF group, but was still present at a substantial level in the HV-DRG1 group.

Fiber-modified HDAd vectors expressing Cre turn on GFP expression in DRG neurons of ROSA-GFP mice. To test whether HDAd containing DRG targeting motifs in the fiber transduce the intended targets, we used ROSA-GFP mice, in which transgenic GFP expression is interrupted by the stop fragment flanked by *loxP* sequences. Upon Cre-mediated excision of the stop fragment, GFP is expressed (Figure 2A). We generated HDAd expressing Cre driven by EF-1 promoter using HV-WF (referred to herein as HDAd-WF-Cre) and then switched vector capsids by coinfection of HDAd-WF-Cre with HV-DRG1, HV-DRG2, HV-DRG3, and HV-KO1S* (Supplemental Figure 1C and Supplemental Figure 2B). We selected the i.t. route for HDAd-mediated gene transfer to the DRG, because i.t. injections are a routine procedure in clinical practice and are associated with negligible side effects when performed judiciously by trained physi-

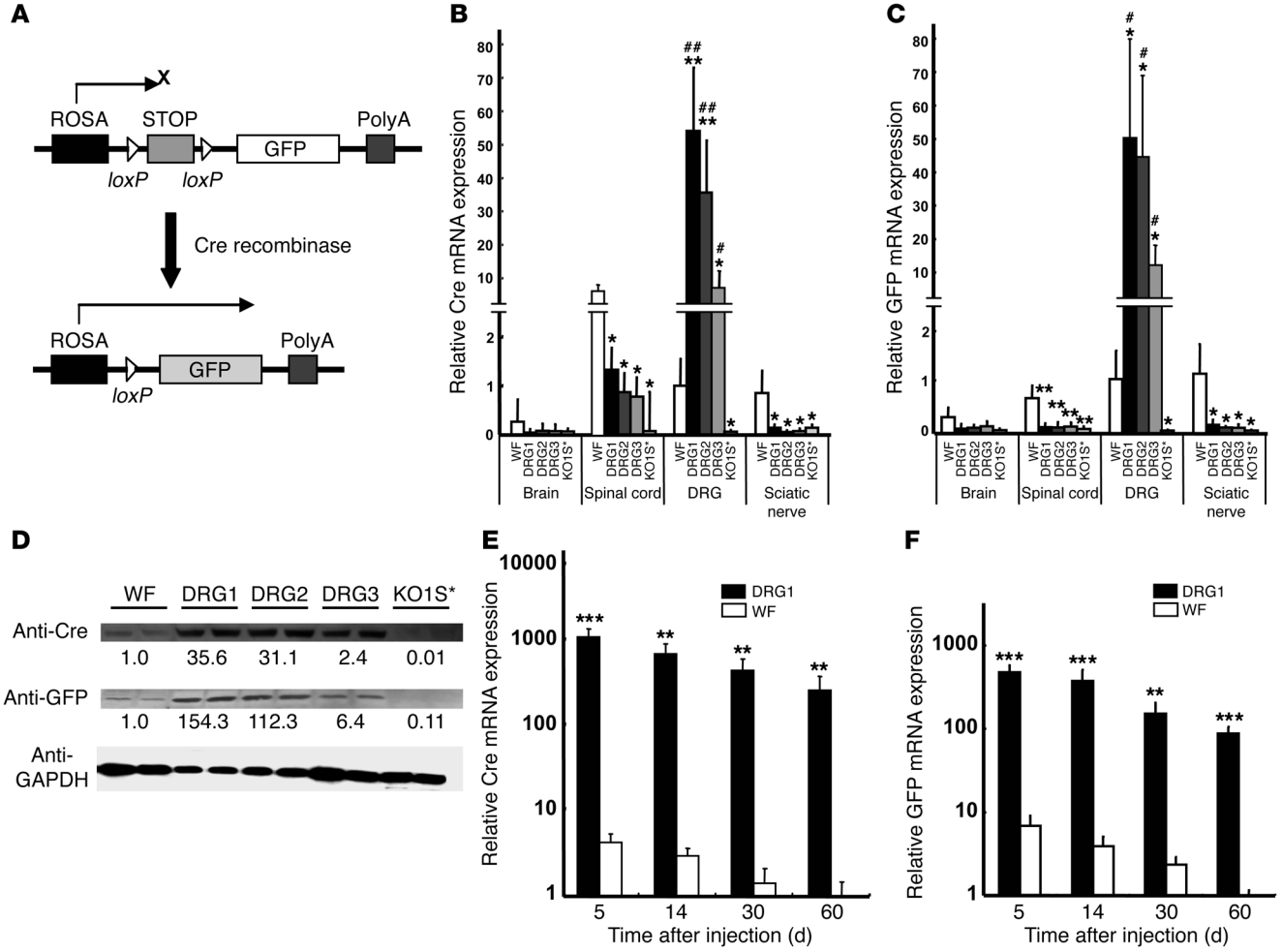

Figure 2

HDAds harboring DRG neuron homing peptides transduce DRG neurons and turn on GFP expression in ROSA-GFP mice. (**A**) Strategy to evaluate targeting tissues in ROSA-GFP mice using fiber-modified HDAd expressing Cre. GFP gene expression is blocked by a STOP fragment flanked by *loxP* sequence. Upon excision of the STOP fragment by Cre, GFP is expressed. Thereby, GFP expression is dependent on HDAd-mediated Cre gene transfer. (**B** and **C**) Cre and GFP mRNA expression in neuronal tissues. Fiber-modified HDAd expressing Cre (1×10^8 vp) were injected i.t. into ROSA-GFP mice. Neuronal tissues were harvested 5 days after injection, and mRNA was quantified by real-time RT-PCR. Results are expressed relative to the HDAd-WF-Cre–treated DRG group. HV contamination in fiber-modified HDAd, determined by real-time PCR, ranged from 0.0007% to 0.037%. (**D**) Immunoblot analysis of Cre and GFP protein expression 5 days after HDAd injection. Band intensities were normalized to GAPDH. Numbers below blots denote protein expression, expressed relative to HDAd-WF-Cre. (**E** and **F**) Long-term Cre and GFP mRNA expression in DRG. HDAd-WF-Cre or HDAd-DRG1-Cre (1×10^8 vp) were injected into ROSA-GFP mice, and Cre and GFP mRNAs in DRG were analyzed at the indicated time points. Results are expressed relative to the day-60 HDAd-WF-Cre group. $^*P < 0.05$, $^{**}P < 0.01$, $^{***}P < 0.001$ versus WF, $^{\#}P < 0.05$, $^{\#\#}P < 0.01$ versus KO1S*. Note the use of log scale in **E** and **F**.

cians. HDAd were injected locally into the subarachnoid space, mice were sacrificed 5 days later, and mRNA expression was determined by real-time RT-PCR. The expression of Cre and GFP in different tissues (Figure 2, B and C) was consistent with the biodistribution of HV (Figure 1, C–E). HDAd-DRG1-Cre–HDAd-DRG3-Cre all expressed Cre and GFP 10- to 50-fold higher than HDAd-WF-Cre in DRG, while HDAd-KO1S*-Cre showed minimal expression. The Cre mRNA level was barely detectable in brain and sciatic nerve. It was generally low in spinal cord, in which tissue the HDAd-WF-Cre led to the highest expression compared with the other tissues and other vectors tested (Figure 2B). GFP mRNA expression was barely detectable in all 3 sites (brain, spinal cord, and sciatic nerve; Figure 2C). Furthermore, very low levels of Cre and GFP mRNA were detected in DRG of the HDAd-WF-Cre–treated group (Figure 2, B and C). In contrast, HDAd-DRG1-Cre–HDAd-DRG3-Cre led to parallel high-level expression of both Cre and GFP mRNA in DRG of injected animals. In all cases, HDAd-KO1S*-Cre–induced expression of Cre and GFP was essentially undetectable. The relative mRNA levels were also reflected by the relative expression of Cre and GFP proteins by immunoblot analysis (Figure 2D). HDAd-DRG1-Cre and HDAd-DRG2-Cre induced 30-fold higher protein levels than HDAd-WF-Cre. Similarly, GFP expression in mice treated with HDAd-DRG1-Cre or HDAd-DRG2-Cre was more than 100-fold higher than that with HDAd-WF-Cre, while it was virtually undetectable in mice treated with HDAd-KO1S*-Cre (Figure 2D). By fluorescent microscopy, GFP fluorescence was readily detected

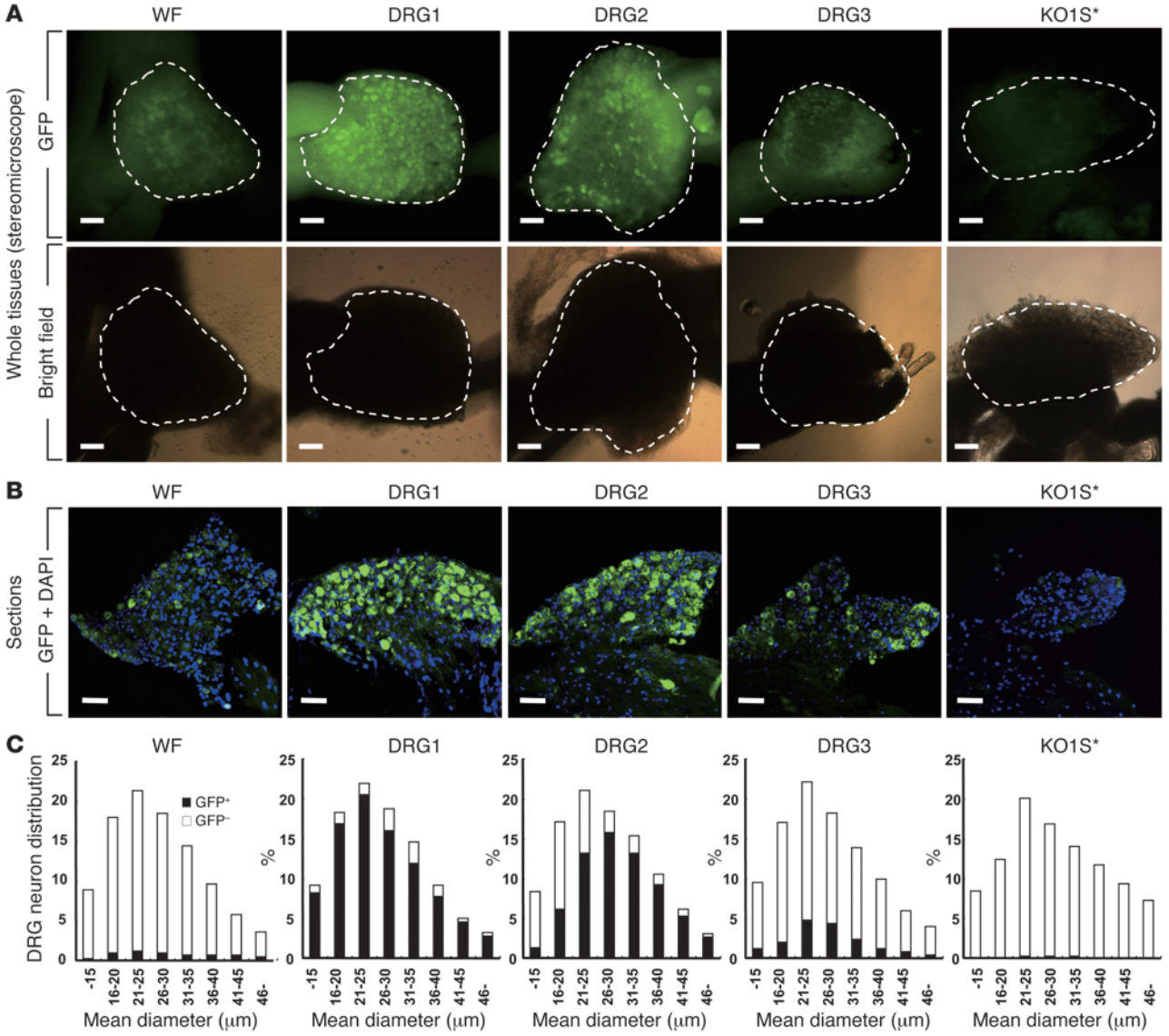

Figure 3
Histological analysis of GFP expression in DRG neurons after transduction with DRG-targeting HDAd vectors. (**A**) GFP expression in whole DRG tissues. Shown are images under GFP filter and bright filter. Dashed lines denote the margin of DRG tissues. (**B**) DRG sections with DAPI nuclear stain. (**C**) Distribution of GFP-positive DRG neurons in each 5 μm of mean diameter. Scale bars: 100 μm.

in individual neurons of DRG transduced by HDAd-DRG1-Cre and HDAd-DRG2-Cre (Figure 3A). HDAd-DRG3-Cre–transduced DRG emitted weak fluorescence; HDAd-WF-Cre also produced detectable but even weaker fluorescence. No fluorescence was detected in the KO1S* group. The proportion of GFP$^+$ to DAPI$^+$ neurons was 88.1% in the HDAd-DRG1-Cre group, 67.7% in the HDAd-DRG2-Cre group, 16.9% in the HDAd-DRG3-Cre group, and 6.3% in the HDAd-WF-Cre group, respectively (Figure 3B). The size distribution of GFP$^+$ cells was generally larger in the HDAd-DRG1-Cre and HDAd-DRG3-Cre groups than in the HDAd-DRG2-Cre group (Figure 3C). A few scattered GFP$^+$ areas were found in the brain and sciatic nerve of the HDAD-WF-Cre group (Supplemental Figure 7, A and C, arrows), while GFP$^+$ areas were identified in the spinal cord at or close to the injection sites in all but the HDAD-KO1S*-Cre group (Supplemental Figure 7B).

HDAds produce long-term transgene expression with markedly attenuated inflammatory response. Transgenes delivered by Ads, including HDAds, are essentially not integrated into the host genome, and their expression decreases with cell turnover. We compared the level of Cre and GFP mRNA expression in the DRG of HDAd-DRG1-Cre– and HDAd-WF-Cre–treated groups. HDAd-WF-Cre treatment led to low-level expression of both at day 5, with rapid decline in relative expression over the next 2 months, such that 22.9% and 14.5% of the initial day-5 mRNA levels remained at day 60 for Cre and GFP, respectively (Figure 2, E and F). In contrast, HDAd-DRG1-Cre–treated DRG led to more than 100-fold higher Cre and GFP expression at day 5. Over the subsequent 2 months, mRNA expression diminished at a greatly reduced rate and was 23.3% for Cre and 18.5% for GFP mRNA at day 60. To further examine both the long-term transgene expression by HDAd and its effect on the host

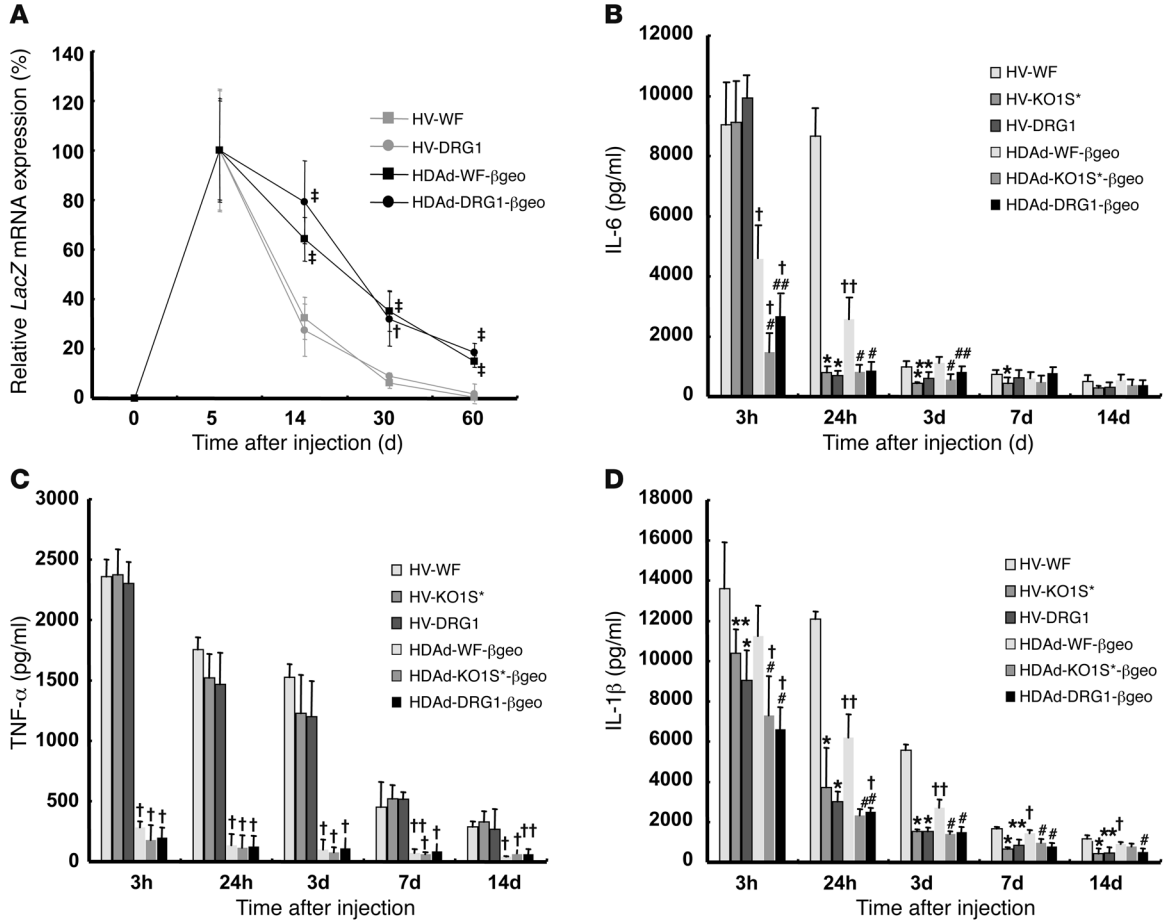

Figure 4

Fiber-modified HDAd supports long-term transgene expression and improves safety profile. (**A**) Long-term expression of *lacZ* gene in DRG. Ad or HDAd vectors (1×10^8 vp) were injected into C57BL/6 wild-type mice, and DRG was isolated at the indicated time points for quantitation of *LacZ* mRNA, normalized to β-actin mRNA. Results are expressed relative to day 5. (**B**–**D**) Targeted HDAd vector induces less inflammation. CSF was collected at the indicated time points, and cytokines IL-6 (**B**), TNF-α (**C**), and IL-1β (**D**) were measured by ELISA. $^{*}P < 0.01$, $^{**}P < 0.05$ versus HV-WF; $^{\#}P < 0.01$, $^{\#\#}P < 0.05$ versus HDAd-WF-βgeo; $^{\ddagger}P < 0.001$, $^{\dagger}P < 0.01$, $^{\dagger\dagger}P < 0.05$ versus respective HV.

inflammatory response, we injected β*geo*-expressing HDAd and HV into mice (Supplemental Figure 2, A and C). We first quantitated *LacZ* mRNA expression for the 2-month period after injection (Figure 4A). Given the arbitrary setting of *LacZ* mRNA day-5 expression as 100%, for both HDAd-WF-βgeo and HDAd-DRG1-βgeo, expression gradually decreased to approximately 20% at day 60. In the corresponding HVs, HV-WF and HV-DRG1, the decline in mRNA was substantially faster, to about 0.4%–1.7% of the initial level at day 60. Thus, the relative stability of transgene expression depends on the vector (lasting substantially longer for HDAd than for HV), and not on the fiber type (WF versus DRG1). We note, however, that HDAd-DRG1-βgeo, which showed 100-fold higher initial *LacZ* expression, was still readily apparent at the end of 60 days, whereas HV-mediated expression was no longer evident. HDAd does not produce any viral proteins, and HDAd-mediated transgene expression is largely free of chronic inflammatory response. Nonetheless, an acute inflammatory response can happen upon HDAd or HV administration as a result of innate immunity. We monitored acute toxicity by measuring cytokines secreted into the CSF and found that IL-6 levels increased 3 hours after vector injection in all groups, but to a much lesser extent in mice treated with HDAd. However, IL-6 production after HDAd-KO1S*-βgeo and HDAd-DRG1-βgeo injection was significantly lower than that after HDAd-WF-βgeo injection (Figure 4B). Although IL-6 expression was still elevated in mice treated with HV-WF 24 hours later, it returned to a level similar to that of PBS treatment (Supplemental Figure 8A) in all other groups, which suggests that attenuation of natural tropism reduces Ad-associated induction of IL-6. The secretion of TNF-α was not influenced by detargeting (Figure 4C and Supplemental Figure 8B). However, the response to HDAd and HV differed markedly: HV produced a robust TNF-α response that lasted at least 2 weeks, while the response to HDAd was greatly attenuated (Figure 4C). The kinetics of CSF IL-1β differed from those of IL-6 or TNF-α (Figure 4D). Importantly, PBS alone increased IL-1β 4-fold at 3 hours after injection and returned to pretreatment level by day 3 (Supplemental Figure 8C). The IL-1β level was elevated in all groups 3 hours after the vector injection. Although the increase of IL-1β in the HV groups was higher than the HDAd groups, the difference, especially at the early 3-hour time point, was much smaller than that observed for IL-6 or TNF-α.

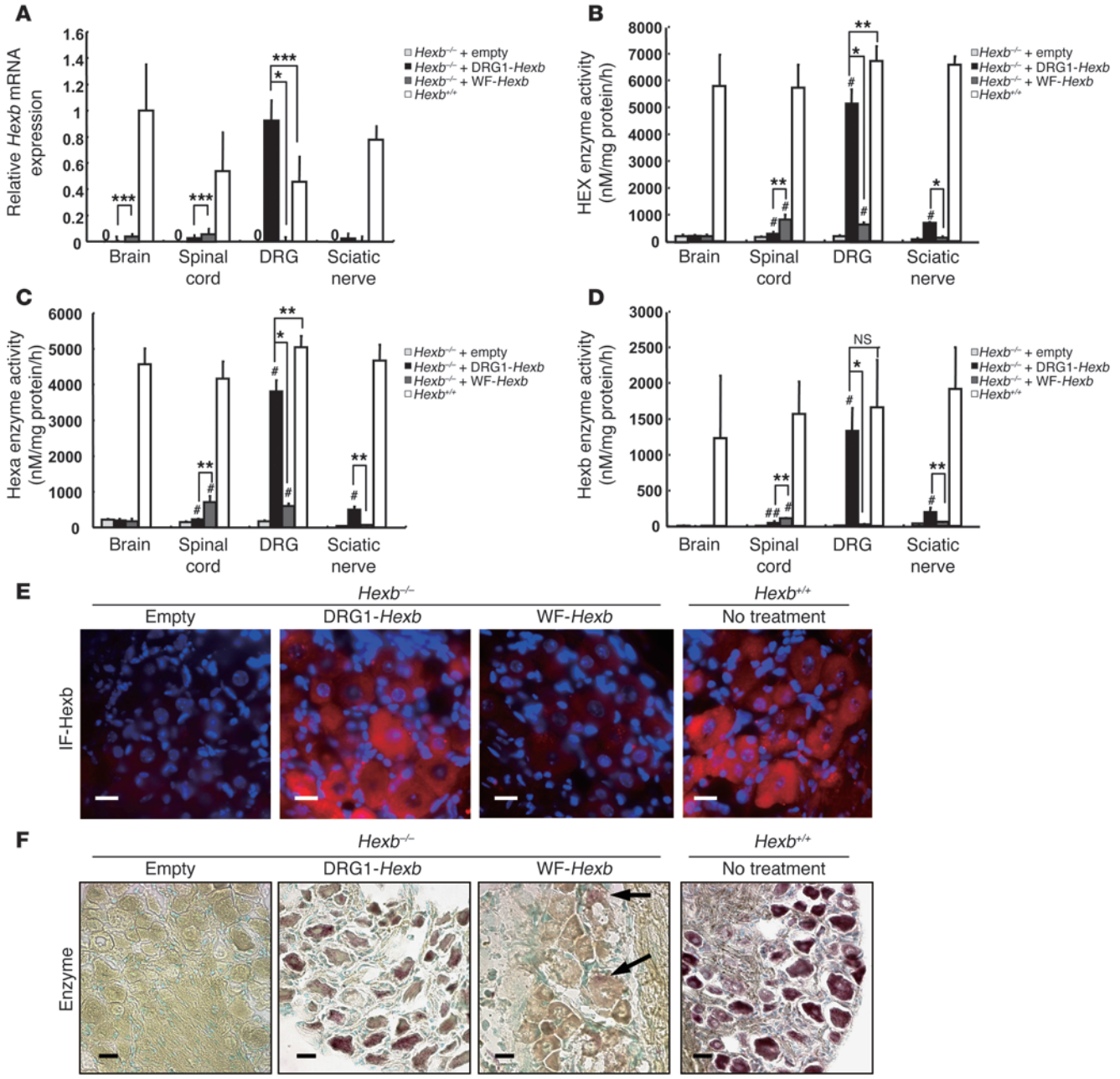

Figure 5

Gene therapy for a mouse model of Sandhoff disease. (**A**) *Hexb* gene expression in neuronal tissues. Various fiber-modified HDAd vectors (1×10^8 vp) were injected into *Hexb*$^{-/-}$ mice through subarachnoid space at the lumbar level, and neuronal tissues were isolated for extraction of cellular RNA 8 weeks after injection. *Hexb* mRNA was quantified by real-time RT-PCR, and expression was calculated relative to that in the brains of wild-type mice. Undetectable expression levels are denoted by "0." (**B**–**D**) Hexosaminidase activities in nervous tissues from wild-type and *Hexb*$^{-/-}$ mice with fiber-modified HDAd vector injection. (**B**) Total hexosaminidase (HEX). (**C**) Hexa. (**D**) Hexb (calculated by subtracting Hexa activity from total hexosaminidase activity). (**E**) Immunofluorescence (IF) for Hexb protein in DRG. (**F**) In situ staining for hexosaminidase activity. Nuclei were stained with methyl green. Arrows indicate weak positive staining in neurons. Scale bars: 20 μm. $^*P < 0.001$; $^{**}P < 0.01$, $^{***}P < 0.05$. $^{\#}P < 0.01$, $^{\#\#}P < 0.05$ versus empty vector–treated *Hexb*$^{-/-}$.

A single injection of DRG-targeting HDAd expressing β-hexosaminidase restores enzyme activity and function of sensory neurons in a mouse model of Sandhoff disease. DRG neurons are involved in many neurological diseases that impair the structural integrity and function of sensory neurons. However, few well-characterized animal models are available to test the effects of restoration of function in sensory neurons. We found that a mouse counterpart of Sandhoff disease in humans was a useful model for this purpose. Sandhoff disease is caused by mutations in the β-hexosaminidase β subunit gene (*HEXB*). Absence of this enzyme subunit leads to defective GM2

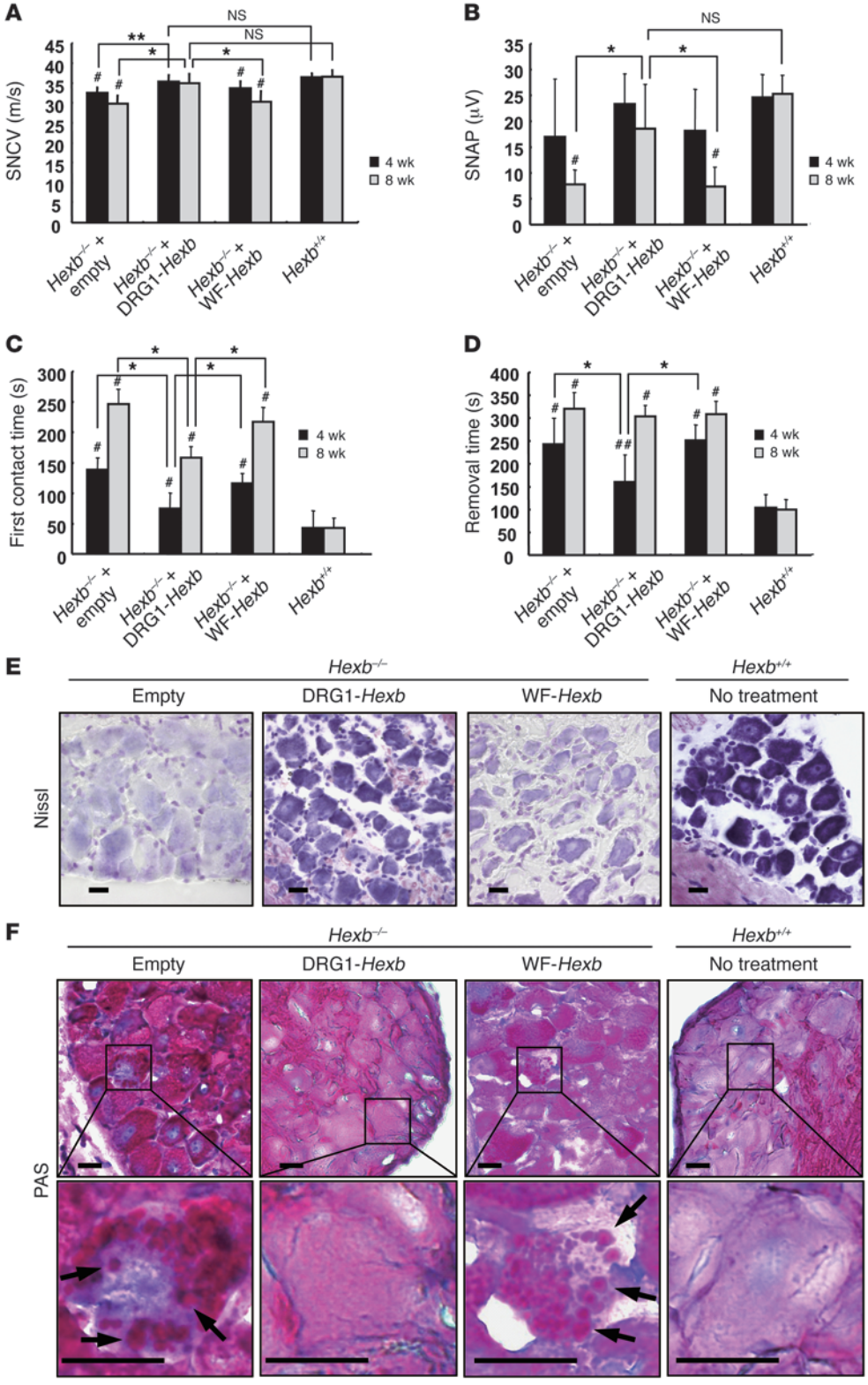

Figure 6
DRG-targeted Hexb expression rescues sensory neuronal responses in *Hexb*$^{-/-}$ mice. Electrophysiological studies and behavior tests were performed at 4 and 8 weeks after treatment. (**A**) SNCV was measured on sural nerve. (**B**) SNAP was recorded in proximal site after stimulation in the distal site at ankle joint. (**C**) First contact time. (**D**) Adhesive removal test. Data are expressed as mean ± SD. $n = 8$ (empty vector); 9 (WF-*Hexb*); 11 (DRG1-*Hexb*); 12 (wild type). (**E**) Nissl stain. (**F**) PAS stain with hematoxylin for nuclear stain. Enlarged views of boxed regions are shown below. Arrows indicate granular formations in neurons. Scale bars: 20 μm. $^{*}P < 0.01$, $^{**}P < 0.05$. $^{\#}P < 0.01$, $^{\#\#}P < 0.05$ versus wild type.

ganglioside degradation and massive accumulation of the ganglioside and other substrates in the lysosomes of neurons. The mouse model for this disease, *Hexb*$^{-/-}$ mice, has previously been shown to develop progressive impairment of motor function (31). Here we found that the DRG of these mice exhibited the typical histopathological changes of GM2 gangliosidosis; furthermore, the animals also displayed abnormal sensory nerve conduction velocity (SNCV) and action potential, objective measurements that can

be used to gauge the severity of the disease. We investigated the effect of DRG neuron–targeted enzyme replacement on the abnormal histology and sensory neuronal impairment in *Hexb*$^{-/-}$ mice. We injected 1×10^8 vp of HDAd vectors expressing *Hexb* driven by the EF-1 promoter into the subarachnoid space of *Hexb*$^{-/-}$ mice at 4 weeks of age and measured mRNA level and enzyme activity in nerve tissues 8 weeks later. An empty vector was used as control. In wild-type mice, all neural tissues expressed *Hexb* mRNA, empty vector–treated *Hexb*$^{-/-}$ mice displayed no detectable *Hexb* mRNA, while *Hexb*$^{-/-}$ mice treated with HDAd-DRG1-*Hexb* (referred to herein as DRG1-*Hexb*) expressed *Hexb* mRNA almost exclusively in DRG, at a level that was significantly higher than that of wild-type mice (Figure 5A). The HDAd-WF-*Hexb* produced *Hexb* mRNA in brain and spinal cord at a level that was substantially lower than that in wild-type mice. Hexa is a heterodimer of α and β subunits, and Hexb is a homodimer of hexosaminidase β subunits. Expression of Hexb rescued both Hexa and Hexb activities in *Hexb*$^{-/-}$ mice. After treatment, total hexosaminidase and Hexa activities in DRG increased to 75%–76% those in wild-type mice (Figure 5, B and C), and Hexb activity was similar to wild-type levels (Figure 5D). The small discrepancies between mRNA level and enzyme activities were probably attributed to the suboptimal ratio of the 2 subunits. As in wild-type mice, Hexb protein expression in DRG neurons in DRG1-*Hexb*–treated *Hexb*$^{-/-}$ mice was confirmed by immunofluorescence, which showed that most DRG neurons were positive for Hexb (Figure 5E). In contrast, immunofluorescence staining was totally absent in the empty vector group and barely detectable in the WF-*Hexb*–treated DRG (Figure 5E). Histochemically, Hex enzyme activity was revealed in the section in situ by a purple-brown coloration resulting from diazonium coupling between fast Garnet GBC and the products catalyzed from naphthol-AS-BI-D-*N*-acetyl-β-glucosaminide by hexosaminidase. In agreement with our enzyme activity data, the histochemical stain in DRG1-*Hexb*–treated mice was present at a level similar to that in wild-type mice, while mice treated with WF-*Hexb* exhibited much lower coupling and those with the empty vector displayed no evident coupling (Figure 5F). Sandhoff disease is a serious gangliosidosis that affects both the central and the peripheral nervous systems and is associated with a much shorter lifespan — we euthanized mice at 16–20 weeks of age because of severe debilitating motor dysfunction. Although DRG1-*Hexb* treatment did not extend the time until euthanasia, progression of objective measures of DRG function was markedly improved by the treatment. The DRG1-*Hexb* group maintained intact SNCV at a normal level 4 and 8 weeks after treatment, while mice treated with empty vector or WF-*Hexb* exhibited significantly impaired SNCV (Figure 6A). Unlike the intact SNCV at 8 weeks in mice treated with DRG1-*Hexb*, the motor nerve conduction velocity (MNCV) deteriorated at similar rates in all treatment groups compared with untreated wild-type controls (Supplemental Figure 9A). Sensory nerve action potential (SNAP) deteriorated markedly in empty vector–treated *Hexb*$^{-/-}$ mice at 8 weeks after treatment (12 weeks of age). The DRG1-*Hexb* treatment group maintained its SNAP at the same level between 4 and 8 weeks, whereas WF-*Hexb* treatment failed to slow the progressive impairment of SNAP in *Hexb*$^{-/-}$ mice (Figure 6B). In contrast, none of the different HDAd treatments could slow the deterioration in compound muscle action potential (CMAP; Supplemental Figure 9B). We performed a functional neurological behavior test by measuring the time needed for the mice to remove an adhesive tape from their hind paw (36). In *Hexb*$^{-/-}$ mice, the time of first contact for tape removal increased progressively with age. Treatment with WF-*Hexb* had no effect on first contact time, while DRG1-*Hexb* treatment significantly shortened this time and slowed deterioration in this parameter at 4 and 8 weeks (Figure 6C). The time required for successful tape removal was also improved by DRG1-*Hexb*, but not WF-*Hexb*, at 4 weeks; however, the beneficial effect of the treatment on this parameter, which depends also on relatively intact motor function, disappeared after 8 weeks (Figure 6D). We investigated the structural integrity of DRG neurons histologically 8 weeks after vector injection. By Nissl staining, DRG neurons in *Hexb*$^{-/-}$ mice treated with DRG1-*Hexb* were similar to those in wild-type mice, although the staining in *Hexb*$^{-/-}$ mice was slightly less intense than in wild-type mice (Figure 6E). This is consistent with the enzyme histochemistry results described above. In contrast, DRG neurons treated with empty vector or WF-*Hexb* showed much lighter staining (Figure 6E), which suggests neuronal degeneration. In periodic acid–Schiff (PAS) staining, granular formation (Figure 6F, arrows) was evident in many DRG neurons in mice treated with the empty or WF-*Hexb* vector, while such accumulation of carbohydrate macromolecules was not detected in the DRG1-*Hexb*–treated and wild-type groups (Figure 6F).

Discussion

Sensory neuronopathies affecting DRG neurons that manifest as pain, hypo- or hyperalgesia, and anesthesia or ataxia can be caused by genetic, nutritional, metabolic, inflammatory, or neoplastic processes. A strategy that enables the efficient delivery of therapeutic transgenes specifically to DRG neurons would represent a significant advance in the treatment of DRG neuronal disorders, because therapeutic measures aimed only at the underlying disease process often fail to reverse the neuronopathy (1, 2).

Our strategy to address this problem was to engineer fiber-modified HDAds that specifically target DRG neurons in vivo. We selected HDAd as the vector because of its large capacity, negligible toxicity, and prolonged transgene expression in the absence of integration, which minimizes its potential tumorigenic effects (37). The target tissue specificity of an HDAd is determined by the specificity of the HV. By using a HV ablated for binding to primary attachment receptors in the fiber (KO1S* mutation) as a platform, we inserted into the HI loop DRG neuron–homing peptides isolated by phage display and biopanning (30). In a previous study, we showed that the presence of the S* mutation at the putative HSPG binding region causes fibers defective at a postinternalization step that lead to poor cellular transduction (34). However, this problem was overcome by incorporating peptide ligands that retargeted the fiber in a manner that allowed for efficient internalization and nuclear trafficking. When we injected the Ad into the subarachnoid space, we found that modified Ad was also detargeted from DRG neurons in vivo. For subgroup C Ad, including Ad5, infection of Ad in vitro occurs first by direct attachment of the fiber to the CAR, then by internalization through α_V integrin via the RGD motif of penton bases or by interaction with HSPG (38). However, i.v. Ad5 directly binds to coagulation factors via interaction between the FX Gla domain and hypervariable regions of the Ad5 hexon surface (22, 23) and is subsequently internalized by binding to LRP and/or HSPG in the liver (21, 24). Koizumi et al. have reported that Ads ablated for binding to CAR, α_V integrin, and HSPG within the FG loop in the fiber knob, as well as Ads that carry a mutation of the AB loop and substitution of the fiber shaft derived from Ad type 35, have markedly reduced tropism to the liver; the modifications also attenuate toxicity, as defined by

IL-6 secretory response after i.v. injection (25). We left the penton and the RGD motif intact, as the RGD motif was thought to be needed for endocytosis and endosomal escape (39, 40). We found that ablation for CAR and HSPG was sufficient to blunt natural tropism. The favorable result obtained in this investigation was, at least in part, due to the direct subarachnoid delivery of the vector, a routine procedure in clinical practice that also eliminates any direct interaction of Ad with blood components. Indeed, this is the first demonstration to our knowledge of efficacy with an in vivo HDAd-targeted gene delivery approach.

Chronic toxicity associated with early-generation Ads has been largely eliminated in HDAd; however, the acute inflammatory response caused by innate immunity against capsid proteins was reported to be similar among the different types of Ad when administered i.v. (41). In the current study, we found markedly reduced IL-6 and TNF-α levels after i.t. HDAd. It is intriguing that the IL-1β response was not greatly attenuated by the HDAds compared with the HVs. An increase in IL-1β is an early response to both Ad and HDAd (41) and is considered to be upstream to IL-6 and TNF-α. In contrast to i.v. administration, i.t. injection of HDAd has previously been reported to invoke neither systemic or local toxicity nor a CNS-specific immune reaction (42). The low toxicity found in the present study may be, at least in part, due to the presence of few immune cells in CSF. Furthermore, the immune response against HDAd might be different between systemic and i.t. injection. Recent reports have shown that the interaction between Ad DNA and TLRs leads to an inflammatory response by the host (reviewed in ref. 43). TLR9 recognizes double-stranded unmethylated CpG DNA, and the response of TLR9 to DNA of mammalian origin may be different from that to viral DNA. The difference in vector genome between HV and HDAd and types of innate immune cells present in the circulation or in the spinal fluid could explain the difference in the host response to the 2 types of vectors. In addition, we found that use of detargeted HDAd-KO1S*-βgeo and HDAd-DRG1-βgeo, which is also based on KO1S*, was associated with a 2-fold reduction of IL-6 at 3 and 24 hours after vector injection, an observation consistent with previous reports showing attenuated cytokine response by Ad detargeted for natural receptors (25).

We tested 3 peptide ligands for their ability to target DRG neurons. DRG1- and DRG3-targeted vectors tended to bind to smaller size neurons than DRG2-targeted vectors. This result was consistent with our previous report, although the surface molecules interacting with these peptides have not been identified (30). HVs containing these peptide ligands increased the efficiency of transduction of DRG neurons in vitro as well as in vivo (Figure 2). DRG1 was the most potent, and transduction of DRG neurons by HV-DRG1 was greater than 100-fold more efficient than transduction by HV-WF. This DRG-targeting HV had a profound effect on transgene expression. *LacZ* expression induced by HV-DRG1 at day 60 was still maintained at a level similar to that induced by HV-WF at day 5. Despite enhanced transduction efficiency of the targeting vector, there was no apparent effect of targeting on decay of transgene expression (Figure 4A). This is not unexpected, however; although tissue or cell targeting plays an important role in efficient transduction, it does not influence intracellular processing or degradation of vector chromosome. Phage display is a powerful technique to identify homing peptides to specific in vivo molecular zip codes. DRG1 appears to support vector internalization and endosome escape, which does not always happen (44). Phage is a small molecule compared with Ad, and the access of bulky Ad particles could be hampered by physical and biological barriers (44). In fact, we found that although i.t. HV-DRG1 efficiently transduced DRG neurons, i.v. HV-DRG1 failed to transduce DRG neurons in vivo (data not shown).

Despite the many human diseases affecting DRG neurons, few mouse models of pure sensory neuron dysfunction are available. We decided to use *Hexb*$^{-/-}$ mice, which exhibit global neurological impairment at 3 months followed by ataxia, bradykinesia, and impaired motor activity and balance. By 18 weeks, hind-limb movement is lost, and they die before 20 weeks (31, 32). As in vivo measurements of sensory function have not to our knowledge been reported in this mouse model, we first documented the occurrence of peripheral sensory impairment in this disorder using sensory nerve conduction studies and mixed sensory/motor function (i.e., tape removal) tests (Figure 6, C and D). A single injection of DRG1-*Hexb* by lumbar puncture into the CSF increased Hex activity in DRG neurons and restored peripheral sensory function, but not motor neuron function, in *Hexb*$^{-/-}$ mice. In histological analysis, Hexb-immunoreactive protein was readily detected in DRG neurons of mice treated with DRG1-*Hexb* but not with WF-*Hexb*. Very little PAS-positive granular formation in the cell body, which represents ganglioside accumulation, was seen in the DRG1-*Hexb*–treated mice. Nissl stain was strongly positive in the DRG1-*Hexb* group, similar to that seen in wild-type mice. It is important to note that DRG1-*Hexb* treatment conferred protection to sensory neuron function but had no detectable effect on motor nerve function. When we assessed nerve function by the tape removal test, deterioration in first contact time was significantly improved by the treatment at both 4 and 8 weeks, because sensory function was dominant in this behavior test. In contrast, the tape removal time, determined by a combination of sensory and motor functions, was partially corrected at 4 weeks, but not at 8 weeks. Despite a marked improvement in SNCV, the behavior tests were still quite abnormal, because performance in these tests requires the presence of intact peripheral and central nervous systems, and our treatment had no effect on the latter. Therefore, use of the *Hexb*$^{-/-}$ mice enabled us to show that DRG neuron–targeted gene therapy specifically restored DRG function without affecting motor nerve, spinal cord, or brain function.

There are many potential clinical applications of the treatment strategy that we developed in this investigation. Neuropathic pain occurs commonly among patients with various metabolic and inflammatory disorders. For example, diabetic neuropathy is the most common chronic complication of diabetes, affecting millions of people in the United States (45). Many of these individuals experience neuropathic pain caused by sensory neuron dysfunction (6). Patients with ganglionopathies caused by autoimmune diseases or drug toxicities also commonly experience severe neuropathic pain (2). Treatment of these and other sensory neuronopathies by i.t. DRG-targeting HDAds that express neurotrophic factors or analgesic peptides may become a new therapeutic option in the future. It has previously been reported that the immune response to foreign material injected i.t. is attenuated (18, 42), which may allow for the repeat administration of HDAd via this route for repeated treatments. We note that HDAd can be administered repeatedly even when it is given by the i.v. route, as long as we use HVs of different serotypes (33, 46). Finally, the nonintegrating nature of HDAd is an advantage in that it minimizes the chance of genotoxicity and induced tumorigenesis (37).

In this study, we developed a strategy to produce HDAds that specifically target DRG neurons. One advantage of this approach is that HDAds expressing a therapeutic gene made by a generic HV could be retargeted to tissues or cell types of interest by amplification with HVs containing targeting ligands. HDAds and fiber-modified HVs were separately produced and combined only at the final amplification step. It is noteworthy that novel targeting peptides are being identified by multiple laboratories (47), and the repository of targeting HVs will expand rapidly, which will allow us to customize HDAd delivery to treat specific diseases and organ systems. Clinical trials using early-generation Ads have been ongoing for years (48, 49). The development of the strategy described herein, using the much more versatile and far less toxic HDAd, should facilitate its possible application in clinical trials for DRG neuronopathies in the near future.

Methods

Cell culture. To generate 293-fiber cells, we used lentiviral vector–mediated gene transfer. Ad5 fiber was subcloned by PCR from AdEasy vector using the following primers: 5′ upstream, 5′-GGATCCG**CCACC**ATGAAGCGCGCAAGACCGTC-3′; 3′ downstream, 5′-GCGGCCGCTTATTCTTGGGCAATGTATG-3′. They contained artificial cloning sites (underline) and the Kozak sequence (bold). The Ad5 fiber cDNA was then subcloned into the pHIV-EF-1-puro, a first-generation self-inactivating vector modified from pHIV-AP (50). LV-Ad5 fiber was produced by cotransfection of LV shuttle vector and pME-VSVG into 293T cells by the standard calcium phosphate precipitation method (Supplemental Figure 3A). The 293-fiber cells were established by selection on puromycin (1 μg/ml). We maintained 293, 293-fiber, and 293Cre66 cells in α-MEM supplemented with 10% FBS and antibiotic-antimicotics (Invitrogen). Puromycin (1 μg/ml) and G418 (0.8 mg/ml) were included in the media for 293-fiber and 293Cre66 cells, respectively. DRG neurons were isolated from C57BL/6 mice 1 day before experiments and cultured under F-12 with 10% FBS, as previous described (30). Infection was performed in nonserum media at 37°C for 30–60 minutes in a CO_2 incubator.

Construction of fiber-modified first-generation HV. To construct fiber-modified HV (Supplemental Figure 1A) using AdEasy system (Stratagene), a 2-kb fragment containing 1.7-kb NdeI/PmeI fragment coding for Ad5 fiber was first subcloned into pCR2.1-TOPO (Invitrogen) by PCR using pDV153-KO1S* as a template, generating pCR2.1-fiber-KO1S*. A derivative of pDV137, pDV153-KO1S* harbors the S* mutation of the putative HSPG-binding region, the KO1 mutation, and the unique BspEI site in the HI loop (Table 1, Figure 1A, and ref. 34). Next, 3 peptide ligands targeting DRG neurons isolated by biopanning of phage display (30) were subcloned into the BspEI site of pCR2.1-fiber-KO1S*, resulting in pCR2.1-DRG1, -DRG2, and -DRG3. The 1.7-kb NdeI/PmeI fragment was excised from these 3 vectors and pCR2.1-fiber-KO1S*, then subcloned into pDV153-KO1S* vector. The 7-kb SpeI/PacI fragment from these 4 clones were subcloned into pAdEasy-1 vector (Stratagene). To make fiber-modified HV, we modified pShuttle (Stratagene) to have the packaging signal (ϕ) flanked by *loxP* sites with the MluI site downstream of the second *loxP* site for cloning purposes (pShuttle-*loxP*-ϕ-*loxP*). To insert 2 reporter genes in HV, we first subcloned both the 5.2-kb βgeo cassette and the 2.2-kb BamHI/BglII fragment of RLCMV (Promega) containing an Rluc expression cassette into pLPBL-1. The resulting dual gene expression cassette was excised by AscI digestion and subcloned into the MluI site of pShuttle-*loxP*-ϕ-*loxP*, creating pShuttle-*loxP*-ϕ-*loxP*-βgeo-RLCMV. HV plasmids were generated by homologous recombination in BJ5183 cells (Stratagene). HV-DRG1, HV-DRG2, HV-DRG3, and HV-KO1S* were produced by transfection into 293-fiber cells. HV-WF was produced on 293 cells. After production of HVs, we tested the excision of the packaging signal by 293Cre66 cells. Infection of 293Cre66 with HVs removed the packaging signal, resulting in a 262-bp PCR product instead of the 460-bp product from the intact HV. The excision of the packaging signal was also confirmed by DNA sequence analysis.

Construction of HDAd vectors. The cDNA of Cre recombinase was cloned by PCR using pBS185 vector (Invitrogen) as template and the following PCR primers: 5′ upstream, 5′-TTAATTAAG**CCACC**ATGTCCAATTTACTGACCGTACAC-3′; 3′ downstream, 5′-GCGGCCGCCTAATCGCCATCTTCCAGCAG-3′. They contained artificial cloning sites (underline) and the Kozak sequence (bold). The *Hexb* cDNA was cloned from C57BL/6 mouse brain into pCR2.1-TOPO (Invitrogen) by RT-PCR using the following primers: 5′ upstream, 5′-ATGCCGCAGTCCCCGCGTA-3′; 3′ downstream, 5′-CTGGAATGCTGTAGACGTCTGTC-3′. These cDNAs were subcloned into pBOS vector that contains EF-1 promoter and rabbit β-globin polyadenylation signal on pLPBL-1 backbone. These expression cassettes and βgeo-RLCMV described above were excised by AscI digestion and then subcloned into pΔ28 vectors (51). All HDAd vectors were first made by a previously published method (37) using HV-WF and 293Cre66 cells (Supplemental Figure 1B). Fiber-modified HDAd vectors were made by coinfection of HDAd vector and fiber-modified HV, as outlined in Supplemental Figure 1. The titer of targeting-HDAd was determined by DNA concentration from purified vector solution (37). HV contamination in HDAds was determined by real-time PCR using the following primers: HV 5′ upstream, 5′-GACCATCAATCTTGACGACC-3′; HV 3′ downstream, 5′-ATGTCGCTTTCCAGAACCC-3′; HDAd 5′ upstream, 5′-CCCATCTCCTTCATCACATCTC-3′; HDAd 3′ downstream, 5′-TCACTCCAGCCTCAACATCC-3′. HV contamination was less than 0.05% in all preparations.

Mice. Male 8- to 12-week-old C57BL/6, B6;129-*Gt (ROSA)26Sor*^{tm2Sho}/J (Rosa-GFP), and *Hexb*$^{+/-}$ mice, a model of Sandhoff disease, were purchased from The Jackson Laboratory. Homozygous *Hexb*$^{-/-}$ and wild-type *Hexb*$^{+/+}$ mice were generated by mating *Hexb*$^{+/-}$ mice, and littermates were used. Genotyping was carried out according to the protocols of The Jackson Laboratory. All animals were housed, fed water and mouse chow ad libitum, and maintained under a 12-hour light/12-hour dark cycle. All experiments were performed according to protocols reviewed and approved by the Institutional Animal Care and Usage Committee at Baylor College of Medicine.

Luciferase assay in vitro and in vivo. For in vitro studies, we plated 293 cells and isolated DRG neurons from C57BL/6 mice 1 day before infection, and infected them with HVs at 1,000 vp/cell. The next day, cells were harvested in a lysis buffer supplied with the luciferase assay kit (Promega), and the lysates were assayed for luciferase activity per the manufacturer's protocol. For in vivo studies, we injected 1×10^8 vp of each vector into mice through subarachnoid space at the lumbar level. Mice were euthanized 5 days after vector treatment, and brain, spinal cord, DRG, and sciatic nerve were isolated. Tissues were homogenized with lysis buffer, and the supernatants were assayed for luciferase activity.

X-gal staining of cells and nervous tissues. For in vitro studies, cells were fixed with fixation solution supplied in β-gal staining kit (Invitrogen) 1 day after infection and incubated with X-gal per the manufacturer's protocol. For in vivo studies, mice were transcardiacally fixed with 4% paraformaldehyde 5 days after vector injection, and isolated nervous tissues were incubated with X-gal for 4 hours. We observed all tissues under standard microscope and stereomicroscope. Several pictures for brain and spinal cord were combined to show the whole central nervous system. Subsequently, 10-μm-thick cryosections were prepared.

Quantitative RT-PCR. Total cellular RNA was extracted by TRIzol (Invitrogen) and treated with DNase I digestion. After reverse transcription using oligo dT, mRNA was quantified by real-time PCR using iQ SYBR Green Supermix (Bio-Rad). The following primers were used: LacZ 5′ upstream, 5′-GTTGCAGTGCACGGCAGATACACTTGCTGA-3′; LacZ 3′

downstream, 5′-GCCACTGGTGGGCCATAATTCAATTCGC-3′; Cre recombinase 5′ upstream, 5′-GCATTACCGGTCGATGCAACGAGTGATGAG-3′; Cre recombinase 3′ downstream, 5′-GAGTGAACGAACCTGGTCGAAATCAGTGCG-3′; GFP 5′ upstream, 5′-GCACGACTTCTTCAAGTCCGCCATGC-3′; GFP 3′ downstream, 5′-GCGGATCTTGAAGTTCACCTTGATGCC-3′; Hexb 5′ upstream, 5′-ACAGTTGCAGAAGCTCCTGGT-3′; Hexb 3′ downstream, 5′-CCTCTATGAGGGAATCTTGGAG-3′; β-actin 5′ upstream, 5′-GACGGCCAGGTCATCACTAT-3′; β-actin 3′ downstream, 5′-CTTCTGCATCCTGTCAGCAA-3′. Detection was carried out with Mx3000P QPCR system (Stratagene), and results were analyzed by MxProQPCR software (version 4.1.0.0; Stratagene). All data were normalized to β-actin values.

Immunoblots. DRG and 293-fiber cells were lysed with RIPA buffer (150 mm NaCl, 2 mm EDTA, 1% Nonidet P-40, 1% sodium deoxycholate, 0.1% SDS, 50 mm NaF, 10 μg/ml aprotinin, 10 μg/ml leupeptin, 1 mm phenylmethylsulfonyl fluoride, and 20 mm Tris-HCl buffer, pH 7.4) and were centrifuged at 12,000 *g* for 20 minutes at 4°C to collect the supernatant. Proteins (20 μg) were separated by 7.5%–15% SDS-PAGE and transferred to a polyvinylidene difluoride filter (Immobilon Millipore). The blots were incubated overnight at 4°C with rabbit anti-Cre antibody (1:1,000; Novagen), mouse monoclonal anti-GFP antibody (1:1,000; BD Biosciences — Clontech), or anti-Ad fiber (1:1,000; ab3233; Abcam). Immunoreactive proteins were detected by enhanced chemiluminescence (PIERCE Biotechnology) after incubation with either horseradish peroxidase–conjugated anti-rabbit Ig or anti-mouse Ig (1:2,000; Bio-Rad).

ELISA for cytokines in CSF. CSF was collected from cistern magna at 3 and 24 hours as well as 3, 7, and 14 days after vector injection. IL-1β, IL-6, and TNF-α levels were determined using an ELISA kit (eBioscience).

Hexosaminidase enzyme assay. Total β-hexosaminidase activity was measured using 4-methylumbelliferyl-2-acetamido-2-deoxy-β-D-glucopyranoside (4-MUG; Sigma-Aldrich) as the substrate. Hexa activity was assayed using 4-methylumbelliferyl-6-sulfo-2-acetamido-2-deoxy-β-D-glucopyranoside (4-MUGS; Calbiochem). Hexb activity was determined by subtracting Hexa activity from total hexosaminidase activity (52). Enzyme activity was expressed as nmol/mg protein/h.

Histological analysis of GFP expression in ROSA-GFP mice. For GFP expression analysis, nervous tissues were directly observed under fluorescent microscope after dissections. The 10-μm cryosections were prepared from DRG and mounted with VECTASHIELD mounting medium with DAPI (Vector Laboratories).

Histological analysis of Hexb$^{-/-}$ mice. Mice were perfused transcardially with cold saline followed by 4% paraformaldehyde, 0.05% glutaraldehyde, 0.5% picric acid, and 0.01 M phosphate buffer (pH 7.4) solution. L1–L5 DRG tissues were removed, and 10-μm-thick cryosections were incubated with goat anti-Hexb antibody (1:100; Santa Cruz Biotechnology Inc.) overnight at 4°C. The next day, sections were incubated with rhodamine-labeled donkey anti-goat IgG and mounted with VECTASHIELD mounting medium with DAPI (Vector Laboratories). Other sections from vector-treated mice were also used for PAS (PAS staining system; Sigma-Aldrich) and Nissl stain with cresyl violet (Sigma-Aldrich). For enzymatic histochemical analysis of hexosaminidase, DRG were immersed in Baker fixative solution (4% paraformaldehyde and 1% anhydrous calcium chloride, pH 7.2) for 1 hour at 4°C, then immersed into gum-sucrose solution (14% antiseptic thymol, 0.14% gum arabic, 1.25 M saccharose) for 24 hours at 4°C. Cryosections (10 μm) were incubated in working solution containing 0.5 mM naphthol-AS-BI-D-*N*-acetyl-β-glucosaminide (Sigma-Aldrich) and 3.6 mM Fast Garnet GBC sulfate salt (Sigma-Aldrich) at pH 5.2 for 30 minutes at 37°C and then counterstained with 1% methyl green for nuclei.

Electrophysiological studies and behavior tests. Nerve conduction studies were performed with CADWELL SIERRA 6200A (Cadwell Laboratories) under anesthetization at temperatures from 30°C to 32°C. The motor nerve conduction study was performed in the sciatic nerves as described previously (53). For sensory nerve conduction studies, sural nerves were stimulated in the distal site at the ankle joint level and were recorded in a proximal site (53). Adhesive removal tests were performed as neurological behavior tests. Small adhesive stimuli (0.25-inch round Avery adhesive labels) were placed on the hind paw of the mouse, and the time to make contact and remove the sticker was recorded. To remove the stickers, animals would use both fore limbs toward their feet and swipe off the stimulus with both fore paws. Each mouse received 3 trials and had an intertrial interval of at least 3 minutes. All testing was performed in the animal's home cage (36).

Statistics. All data are expressed as mean ± SD. All in vitro experiments were performed in triplicate in at least 3 independent experiments. In vivo analyses were performed using 5 mice per group, unless otherwise specified. Student's unpaired 2-tailed *t* test was used to calculate statistical significance for differences between 2 groups. For multiple data sets, 1-way ANOVA and Scheffe's test were used. A *P* value less than 0.05 was considered significant.

Acknowledgments

We thank Buras Eric, Saya Kanehira, and Michiru Tokura for intellectual and technical assistance and Leslie Wu for manuscript preparation. This study was supported by NIH grants HL-51586, DK-68037 (to L. Chan), and HL-73144 (to K. Oka). A.B. Kritz and A.H. Baker were supported by the Medical Research Council, United Kingdom. T. Terashima was supported in part by a postdoctoral fellowship for study abroad from the Uehara Memorial Foundation, Japan. L. Chan was also supported by the Betty Rutherford Chair from St. Luke's Episcopal Hospital (Houston, Texas, USA).

Received for publication February 25, 2009, and accepted in revised form April 29, 2009.

Address correspondence to: Lawrence Chan, Department of Medicine, Baylor College of Medicine, One Baylor Plaza, Houston, Texas 77030, USA. Phone: (713) 798-4478; Fax: (713) 798-8764; E-mail: lchan@bcm.tmc.edu.

1. Sghirlanzoni, A., Pareyson, D., and Lauria, G. 2005. Sensory neuron diseases. *Lancet Neurol.* **4**:349–361.
2. Kuntzer, T., Antoine, J.C., and Steck, A.J. 2004. Clinical features and pathophysiological basis of sensory neuronopathies (ganglionopathies). *Muscle Nerve.* **30**:255–268.
3. Swanson, A.G., Buchan, G.C., and Alvord, E.C., Jr. 1965. Anatomic changes in congenital insensitivity to pain. Absence of small primary sensory neurons in ganglia, roots, and Lissauer's tract. *Arch. Neurol.* **12**:12–18.
4. Malinow, K., et al. 1986. Subacute sensory neuronopathy secondary to dorsal root ganglionitis in primary Sjogren's syndrome. *Ann. Neurol.* **20**:535–537.
5. Montpetit, V.J., Clapin, D.F., Tryphonas, L., and Dancea, S. 1988. Alteration of neuronal cytoskeletal organization in dorsal root ganglia associated with pyridoxine neurotoxicity. *Acta Neuropathol.* **76**:71–81.
6. Yasuda, H., et al. 2003. Diabetic neuropathy and nerve regeneration. *Prog. Neurobiol.* **69**:229–285.
7. Wanschitz, J., Hainfellner, J.A., Kristoferitsch, W., Drlicek, M., and Budka, H. 1997. Ganglionitis in paraneoplastic subacute sensory neuronopathy: a morphologic study. *Neurology.* **49**:1156–1159.
8. Terenghi, G. 1999. Peripheral nerve regeneration and neurotrophic factors. *J. Anat.* **194**:1–14.
9. Chattopadhyay, M., et al. 2005. HSV-mediated gene transfer of vascular endothelial growth factor to dorsal root ganglia prevents diabetic neuropathy. *Gene Ther.* **12**:1377–1384.
10. Wang, X., et al. 2005. Gene transfer to dorsal root ganglia by intrathecal injection: effects on regeneration of peripheral nerves. *Mol. Ther.* **12**:314–320.
11. Jackson, C.A., Messinger, J., Palmer, M.T., Peduzzi, J.D., and Morrow, C.D. 2003. Gene expression in the muscle and central nervous system following intramuscular inoculation of encapsidated or naked poliovirus replicons. *Virology.* **314**:45–61.
12. Xu, Y., Gu, Y., Wu, P., Li, G.W., and Huang, L.Y. 2003. Efficiencies of transgene expression in nociceptive neurons through different routes of deliv-

ery of adeno-associated viral vectors. *Hum. Gene Ther.* **14**:897–906.
13. Glatzel, M., et al. 2000. Adenoviral and adeno-associated viral transfer of genes to the peripheral nervous system. *Proc. Natl. Acad. Sci. U. S. A.* **97**:442–447.
14. Driesse, M.J., et al. 2000. Intra-CSF administered recombinant adenovirus causes an immune response-mediated toxicity. *Gene Ther.* **7**:1401–1409.
15. Waehler, R., Russell, S.J., and Curiel, D.T. 2007. Engineering targeted viral vectors for gene therapy. *Nat. Rev. Genet.* **8**:573–587.
16. Seiler, M.P., Cerullo, V., and Lee, B. 2007. Immune response to helper dependent adenoviral mediated liver gene therapy: challenges and prospects. *Curr. Gene Ther.* **7**:297–305.
17. Brunetti-Pierri, N., and Ng, P. 2008. Progress and prospects: gene therapy for genetic diseases with helper-dependent adenoviral vectors. *Gene Ther.* **15**:553–560.
18. Muruve, D.A., et al. 2004. Helper-dependent adenovirus vectors elicit intact innate but attenuated adaptive host immune responses in vivo. *J. Virol.* **78**:5966–5972.
19. Bergelson, J.M., et al. 1997. Isolation of a common receptor for Coxsackie B viruses and adenoviruses 2 and 5. *Science.* **275**:1320–1323.
20. Tomko, R.P., Xu, R., and Philipson, L. 1997. HCAR and MCAR: the human and mouse cellular receptors for subgroup C adenoviruses and group B coxsackieviruses. *Proc. Natl. Acad. Sci. U. S. A.* **94**:3352–3356.
21. Parker, A.L., et al. 2006. Multiple vitamin K-dependent coagulation zymogens promote adenovirus-mediated gene delivery to hepatocytes. *Blood.* **108**:2554–2561.
22. Waddington, S.N., et al. 2008. Adenovirus serotype 5 hexon mediates liver gene transfer. *Cell.* **132**:397–409.
23. Kalyuzhniy, O., et al. 2008. Adenovirus serotype 5 hexon is critical for virus infection of hepatocytes in vivo. *Proc. Natl. Acad. Sci. U. S. A.* **105**:5483–5488.
24. Shayakhmetov, D.M., Gaggar, A., Ni, S., Li, Z.Y., and Lieber, A. 2005. Adenovirus binding to blood factors results in liver cell infection and hepatotoxicity. *J. Virol.* **79**:7478–7491.
25. Koizumi, N., et al. 2006. Modified adenoviral vectors ablated for coxsackievirus-adenovirus receptor, alphav integrin, and heparan sulfate binding reduce in vivo tissue transduction and toxicity. *Hum. Gene Ther.* **17**:264–279.
26. Hotta, Y., Honda, T., Naito, M., and Kuwano, R. 2003. Developmental distribution of coxsackie virus and adenovirus receptor localized in the nervous system. *Brain Res. Dev. Brain Res.* **143**:1–13.
27. Mizuguchi, H., and Hayakawa, T. 2004. Targeted adenovirus vectors. *Hum. Gene Ther.* **15**:1034–1044.
28. Biermann, V., et al. 2001. Targeting of high-capacity adenoviral vectors. *Hum. Gene Ther.* **12**:1757–1769.
29. Wang, H., et al. 2005. A capsid-modified helper-dependent adenovirus vector containing the beta-globin locus control region displays a nonrandom integration pattern and allows stable, erythroid-specific gene expression. *J. Virol.* **79**:10999–11013.
30. Oi, J., et al. 2008. Isolation of specific peptides that home to dorsal root ganglion neurons in mice. *Neurosci. Lett.* **434**:266–272.
31. Sango, K., et al. 1995. Mouse models of Tay-Sachs and Sandhoff diseases differ in neurologic phenotype and ganglioside metabolism. *Nat. Genet.* **11**:170–176.
32. Sango, K., Yamanaka, S., Ajiki, K., Tokashiki, A., and Watabe, K. 2002. Lysosomal storage results in impaired survival but normal neurite outgrowth in dorsal root ganglion neurones from a mouse model of Sandhoff disease. *Neuropathol. Appl. Neurobiol.* **28**:23–34.
33. Kim, I.H., Jozkowicz, A., Piedra, P.A., Oka, K., and Chan, L. 2001. Lifetime correction of genetic deficiency in mice with a single injection of helper-dependent adenoviral vector. *Proc. Natl. Acad. Sci. U. S. A.* **98**:13282–13287.
34. Kritz, A.B., et al. 2007. Adenovirus 5 fibers mutated at the putative HSPG-binding site show restricted retargeting with targeting peptides in the HI loop. *Mol. Ther.* **15**:741–749.
35. Smith, T.A., et al. 2003. Adenovirus serotype 5 fiber shaft influences in vivo gene transfer in mice. *Hum. Gene Ther.* **14**:777–787.
36. Fleming, S.M., et al. 2004. Early and progressive sensorimotor anomalies in mice overexpressing wild-type human alpha-synuclein. *J. Neurosci.* **24**:9434–9440.
37. Oka, K., and Chan, L. 2005. Helper-dependent adenoviral vectors. In *Current protocols in molecular biology*. John Wiley & Sons Inc. Hoboken, New Jersey, USA. 16.24.11–16.24.23.
38. Dechecchi, M.C., et al. 2001. Heparan sulfate glycosaminoglycans are receptors sufficient to mediate the initial binding of adenovirus types 2 and 5. *J. Virol.* **75**:8772–8780.
39. Wickham, T.J., Mathias, P., Cheresh, D.A., and Nemerow, G.R. 1993. Integrins alpha v beta 3 and alpha v beta 5 promote adenovirus internalization but not virus attachment. *Cell.* **73**:309–319.
40. Shayakhmetov, D.M., Eberly, A.M., Li, Z.Y., and Lieber, A. 2005. Deletion of penton RGD motifs affects the efficiency of both the internalization and the endosome escape of viral particles containing adenovirus serotype 5 or 35 fiber knobs. *J. Virol.* **79**:1053–1061.
41. McCaffrey, A.P., et al. 2008. The host response to adenovirus, helper-dependent adenovirus, and adeno-associated virus in mouse liver. *Mol. Ther.* **16**:931–941.
42. Butti, E., et al. 2008. Absence of an intrathecal immune reaction to a helper-dependent adenoviral vector delivered into the cerebrospinal fluid of non-human primates. *Gene Ther.* **15**:233–238.
43. Huang, X., and Yang, Y. 2009. Innate immune recognition of viruses and viral vectors. *Hum. Gene Ther.* **20**:293–301.
44. Fechner, H., et al. 1999. Expression of coxsackie adenovirus receptor and alphav-integrin does not correlate with adenovector targeting in vivo indicating anatomical vector barriers. *Gene Ther.* **6**:1520–1535.
45. Sadosky, A., McDermott, A.M., Brandenburg, N.A., and Strauss, M. 2008. A review of the epidemiology of painful diabetic peripheral neuropathy, postherpetic neuralgia, and less commonly studied neuropathic pain conditions. *Pain Pract.* **8**:45–56.
46. Morral, N., et al. 1999. Administration of helper-dependent adenoviral vectors and sequential delivery of different vector serotype for long-term liver-directed gene transfer in baboons. *Proc. Natl. Acad. Sci. U. S. A.* **96**:12816–12821.
47. Hajitou, A., Pasqualini, R., and Arap, W. 2006. Vascular targeting: recent advances and therapeutic perspectives. *Trends Cardiovasc. Med.* **16**:80–88.
48. Tolcher, A.W., et al. 2006. Phase I, pharmacokinetic, and pharmacodynamic study of intravenously administered Ad5CMV-p53, an adenoviral vector containing the wild-type p53 gene, in patients with advanced cancer. *J. Clin. Oncol.* **24**:2052–2058.
49. Chiocca, E.A., et al. 2008. A phase I trial of Ad.hIFN-beta gene therapy for glioma. *Mol. Ther.* **16**:618–626.
50. Sutton, R.E., Wu, H.T., Rigg, R., Bohnlein, E., and Brown, P.O. 1998. Human immunodeficiency virus type 1 vectors efficiently transduce human hematopoietic stem cells. *J. Virol.* **72**:5781–5788.
51. Oka, K., et al. 2001. Long-term stable correction of low-density lipoprotein receptor-deficient mice with a helper-dependent adenoviral vector expressing the very low-density lipoprotein receptor. *Circulation.* **103**:1274–1281.
52. Yamaguchi, A., et al. 2003. Plasmid-based gene transfer ameliorates visceral storage in a mouse model of Sandhoff disease. *J. Mol. Med.* **81**:185–193.
53. Terashima, T., et al. 2005. The fusion of bone-marrow-derived proinsulin-expressing cells with nerve cells underlies diabetic neuropathy. *Proc. Natl. Acad. Sci. U. S. A.* **102**:12525–12530.